PHYSICAL REVIEW B **90**, 220104(R) (2014)

Nanoscale phase quantification in lead-free $(Bi_{1/2}Na_{1/2})TiO_3$-$BaTiO_3$ relaxor ferroelectrics by means of ^{23}Na NMR

Pedro B. Groszewicz,[1] Hergen Breitzke,[1] Robert Dittmer,[2] Eva Sapper,[2] Wook Jo,[3] Gerd Buntkowsky,[1,*] and Jürgen Rödel[2,†]

[1]*Institute of Physical Chemistry, Technische Universität Darmstadt, 64287 Darmstadt, Germany*

[2]*Department of Materials Science, Technische Universität Darmstadt, 64287 Darmstadt, Germany*

[3]*School of Materials Science and Engineering, Ulsan National Institute of Science and Technology, 689-798 Ulsan, Republic of Korea*

(Received 3 September 2014; revised manuscript received 5 December 2014; published 24 December 2014)

We address the unsolved question on the structure of relaxor ferroelectrics at the atomic level by characterizing lead-free piezoceramic solid solutions $(100-x)(Bi_{1/2}Na_{1/2})TiO_3$-$xBaTiO_3$ (BNT-xBT) (for $x = 1, 4, 6$, and 15). Based on the relative intensity between spectral components in quadrupolar perturbed ^{23}Na nuclear magnetic resonance, we present direct evidence of the coexistence of cubic and polar local symmetries in these relaxor ferroelectrics. In addition, we demonstrate how the cubic phase vanishes whenever a ferroelectric state is induced, either by field cooling or changing the dopant amount, supporting the relation between this cubic phase and the relaxor state.

DOI: 10.1103/PhysRevB.90.220104 PACS number(s): 77.80.Jk, 76.60.−k

Relaxor ferroelectrics have been intensively studied in the past 30 years because of their intriguing structural and dielectric features [1–3]. Despite that, the nature of their ground state remains an open question [4–12]. Several models have been proposed to describe this puzzling class of materials [1,5–8,13], two of which are mainly concerned with the structure of the ground state of relaxors [4].

The random field (RF) model proposes a single-phase structure broken up into ferroelectric nanodomains. These nanodomains are kept small under the constraint of quenched random electric fields which originate from chemical disorder [7,14]. The other model introduced the concept of "polar nanoregions" (PNRs) [13]. When relaxors are cooled below the Burns temperature, small and randomly oriented polarized regions (PNRs) appear within the otherwise nonpolar crystal structure. Upon further cooling, PNRs grow in size and number [11], but their percolation is prevented by structural disorder and random electric fields [8,10,12]. This behavior would imply the coexistence of PNRs and a nonpolar matrix, in contrast to the single-phase structure proposed by the RF model.

An induced ferroelectric state can be established in relaxors when a strong electric field is applied. This state features macroscopic polarization and breaking of the cubic average symmetry [5,11,15–17]. While the RF model suggests that this transformation and the formation of macroscopic ferroelectric domains are caused only by reorientation of previously nanometric ferroelectric domains, an additional mechanism is required when PNRs are considered. In that case, a long-range ferroelectric state can only be established if the nonpolar matrix becomes polarized, being incorporated by the growing PNRs.

Two questions are raised by contrasting these two models: (1) Does the microscopic structure of relaxor ferroelectrics consist only of ferroelectric nanodomains or do regions of lower local symmetry (PNRs) coexist with a nonpolar matrix of undistorted structure? (2) How does the microscopic structure of relaxors evolve upon electric poling?

In spite of their relevance, such questions have remained unsolved largely because the structural characterization of relaxors is a challenging matter. The distortions from the ideal perovskite unit cell are often small [18], posing difficulties for diffraction techniques to clearly assign a defined symmetry, e.g., in $(Bi_{1/2}Na_{1/2})TiO_3$ (BNT) [18,19]. Solid solutions, especially at the morphotropic phase boundary (MPB), complicate the matter further due to the coexistence of different symmetries. If doped with a barium content of around 6% and 7% [20], BNT-xBT appears cubic to x-ray diffraction [21–23]. Contrastingly, weak superlattice reflections in neutron diffraction suggest the presence of a lower symmetry [23,24]. This contradiction exposes the need for different methods to characterize these materials. Transmission electron microscopy (TEM) and selected area electron diffraction (SAED) have also been employed to characterize the structure at a microscopic scale. Nevertheless, they have only pointed out the same phase coexistence between $R3c$ and $P4bm$ symmetries [12,25], and as other diffraction techniques, they deliver only an averaged picture of the local structure. Such diffraction techniques require a long coherence length, of several hundreds of unit cells. In order to overcome that, diffuse scattering [26–29] has been utilized. Although the nanometric nature of polarized regions was demonstrated, the question on the models cited above has not yet been settled.

A complementary method should address the very local structure in order to search for the origin of polarization, while being able to discern between different local symmetries. Nuclear magnetic resonance (NMR) of quadrupolar nuclei such as ^{23}Na is an appropriate tool for local structure characterization, as the quadrupolar interaction scales with $1/r^3$ [30,31]. Since this interaction responds to electric field gradients (EFGs) on the nucleus' site, this technique can differentiate local symmetries on the nanoscale [32–34].

Solid solutions of composition $(100-x)(Bi_{1/2}Na_{1/2})TiO_3$-$xBaTiO_3$ (BNT-xBT) were chosen for this study. The phase diagram of BNT-xBT [20] encompasses both variations in relaxor character and crystal structure with barium content [3,12,35,36]. Specifically, a rhombohedral

*gerd.buntkowsky@chemie.tu-darmstadt.de
†roedel@ceramics.tu-darmstadt.de

region (barium content, $x < 5$), such as BNT-1BT and BNT-4BT, present relaxor features to some extent [35,37]. Compositions in the transition region ($5 < x < 8$) display strong relaxor features and contain a morphotropic phase boundary. Here these are well represented by BNT-6BT [16]. A tetragonal region ($x > 8$) is represented by BNT-15BT, which is spontaneously ferroelectric at room temperature.

Bulk ceramic samples with a nominal BNT-xBT ($x = 1, 4, 6,$ and 15) composition were prepared by a standard solid-state route [38]. Samples were electrically poled by field cooling from 150 °C to room temperature at 2.8 kV/mm. For annealing they were heated at 2 K/min and kept at 400 °C for 2 h. The temperature-dependent dielectric permittivity $\varepsilon(T)$ of unpoled and poled samples was determined with an HP 4284A at a heating rate of 2 K/min in the frequency range from 100 Hz to 1 MHz.

^{23}Na solid-state NMR spectra were recorded with a Varian Infinity+ 600 MHz spectrometer. Cylindrical ceramic samples were spun at 10 kHz in a 5 mm MAS Varian XYH probe head tuned at 158.75 MHz. A single-pulse experiment with a pulse length of 1.0 μs, a recycle delay of 500 ms, and a dwell time of 0.13 μs ensured appropriate excitation and recording of the spectra. The response function of the NMR probe is slightly asymmetric, which results in an apparent shift of the satellite's maximum away from the center band. For this reason the quantitative signal analysis was assured by reference spectra of simple sodium salts.

The quadrupolar interaction affords ^{23}Na solid-state NMR sensitivity to a material's structure at an atomic level. It consists of an electrostatic interaction between the nuclear quadrupolar moment and the EFG, a structural parameter determined by the local structure. The effect of this interaction on the frequency of each $(m,m-1)$ NMR transition of ^{23}Na ($I = 3/2$) can be described by first-order perturbation theory, and results in the following equation if an axial symmetric EFG tensor is considered [30,31]:

$$\nu_{m,\,m-1} = \nu_L - \frac{eQV_{ZZ}}{8}(3\cos^2\theta - 1)[m^2 - (m-1)^2]. \quad (1)$$

Here, m is the magnetic quantum number, ν_L the unperturbed Larmor frequency, eQ the nuclear quadrupolar moment, V_{ZZ} a measure of the magnitude of the EFG, and θ the angle between the symmetry axis of the EFG tensor and the equipment's external magnetic field.

The last term of Eq. (1) vanishes for $m = 1/2$, hence the $(1/2,-1/2)$ transition is not affected by the quadrupolar interaction and results in a narrow and intense component at ν_L, termed the central transition. In contrast, the frequencies of transitions $(3/2,1/2)$ and $(-1/2,-3/2)$ are shifted symmetrically away from the central one, and are therefore called satellite transitions. Because of their orientation dependence, the satellite transitions merge into a broad component for nonoriented solids (e.g., ceramics). Due to magic angle spinning (MAS), this otherwise broad component splits into a series of narrower peaks [39,40], called the spinning sideband envelope (SSE). Under these conditions the central component is called the center band (CB). The width of the SSE is proportional to V_{ZZ} and can serve as a direct measure for the departure from an ideal cubic local structure. Thus, its observation provides a fingerprint for local breaking of cubic symmetry [32,41].

The intensity ratio between these two spectral components ($I_{\mathrm{SSE}}/I_{\mathrm{CB}}$) is determined by the transition probability of the corresponding transitions, which is proportional to $|\langle m|\, I_x\, |m-1\rangle|^2$ [30]. This expression results in a transition probability of 0.3 for each satellite and 0.4 for the central transition. Accordingly, the $I_{\mathrm{SSE}}/I_{\mathrm{CB}}$ ratio is determined to be equal to 1.5.

This ratio is only valid if the whole sample displays a noncubic local symmetry around the sodium nuclei. For the special case of a cubic local structure, EFG-tensor components vanish ($V_{ZZ} = 0$) and only a single resonance line should be observed in ^{23}Na NMR spectra, as both central and satellite transitions present the same resonance frequency (Eq. (1)).

If cubic and noncubic local symmetries coexist in the same sample, the $I_{\mathrm{SSE}}/I_{\mathrm{CB}}$ ratio falls below 1.5, as the cubic phase contributes signal intensity only to the center band. If I_{SSE} and I_{CB} are the integrals of the spinning sideband envelope and the center band, respectively, one can determine the percentage of the cubic phase content by means of Eq. (2) (see the Supplemental Material for its derivation [42]):

$$\text{cubic } \% = 100\frac{1.5 - \left(\frac{I_{\mathrm{SSE}}}{I_{\mathrm{CB}}}\right)}{1.5 + 1.5\left(\frac{I_{\mathrm{SSE}}}{I_{\mathrm{CB}}}\right)}. \quad (2)$$

In order to validate this relation, the NMR spectra of the reference sodium salts ($NaNO_3$ and $NaNO_2$) were analyzed. These salts display a single, well-defined, noncubic local environment for ^{23}Na in their structure [39], and should, therefore, exhibit an $I_{\mathrm{SSE}}/I_{\mathrm{CB}}$ ratio close to the theoretical value of 1.5. Values of 1.43 and 1.39 were observed for each salt, respectively, which lie within a margin of 7% from the limiting value. Good agreement was also observed when applying Eq. (2), as the cubic content determined for these salts was below 3%. This value can be attributed to the nonideal NMR probe response function and was considered the experimental uncertainty for the quantification of cubic and noncubic phases in ceramic samples.

The ^{23}Na MAS NMR spectrum of unpoled BNT-6BT [Fig. 1(a)] provides an SSE which resembles a broad Gaussian without the characteristic spectral features of a single well-defined quadrupolar interaction tensor [30,39]. Hence, it reflects a distribution in the magnitude of components from the EFG tensor [43], which indicates partial disorder in the local structure of this material.

According to Eq. (1), the observation of the satellite transitions, indicated by the SSE, provides clear evidence for breaking of the local cubic symmetry [32,41]. It indicates that unpoled BNT-6BT is polar at a local scale, despite being macroscopically cubic. The fact that this polar phase is hardly detected macroscopically [21,23,24,35] strongly supports its nanometric character. Moreover, it unveils NMR as a suitable tool for characterizing this class of materials.

^{23}Na NMR not only highlights the polar nature of the local structure but also indicates the presence of a cubic phase for the unpoled state of BNT-6BT. The $I_{\mathrm{SSE}}/I_{\mathrm{CB}}$ ratio of this sample equals to 0.80 (Table I), which is much lower than the limiting ratio of 1.5. Such a low value could be accounted for by the presence of a cubic phase [Fig. 1(c) schematic].

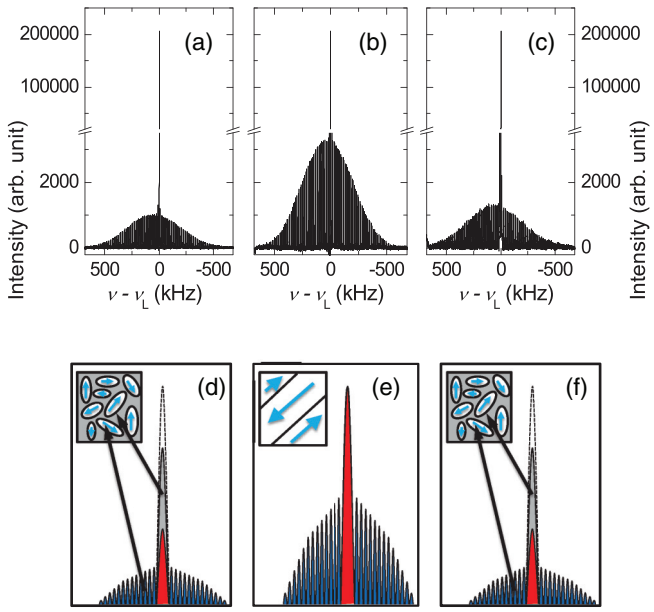

FIG. 1. (Color online) Comparison between (a)–(c) measured and (d)–(f) schematic ^{23}Na MAS NMR spectra of BNT-6BT for different poling states. While the relaxor state [(d), (f)] is observed for (a) unpoled and (c) thermally annealed samples, the induced ferroelectric state (e) corresponds to the poled sample (b). In (a), (d) the overall I_{SSE}/I_{CB} intensity ratio falls below 1.5 due to the presence of a cubic phase (in gray), which contributes intensity only to the center band. SSE's intensity increases and the I_{SSE}/I_{CB} ratio approaches a theoretical value of 1.5 after electric poling [(b), (e)].

Employing Eq. (2), a cubic local symmetry was assigned to ca. 25% of the structure, whereas the remaining 75% display a polar (noncubic) local structure.

Comparison of the NMR spectra of BNT-6BT before and after poling [Figs. 1(a) and 1(b), respectively] reveals a pronounced growth in the SSE intensity. The I_{SSE}/I_{CB} ratio increases from 0.80 for the unpoled to 1.42 for the poled sample (Table I). This change implies that the relative amount of the polar phase increased as a consequence of electric poling. The fact that the I_{SSE}/I_{CB} ratio approached the theoretical value of 1.5 for the poled sample indicates that the polar phase spread throughout most of the structure [Fig. 1(e) schematic]. With the aid of Eq. (2) we could determine that the cubic phase content

TABLE I. I_{SSE}/I_{CB} ratio, SSE width, and ΔT_m for BNT-xBT with different barium content (x) for unpoled and poled samples are contrasted.

	SSE/CB ratio		SSE width (MHz)		ΔT_m (°C)[a]
x (%)	Unpoled	Poled	Unpoled	Poled	Unpoled
1	1.07	1.43	0.64	0.65	25
4	1.31	1.37	0.57	0.57	14
6	0.80	1.42	0.59	0.54	43
15	1.45	1.42	0.39	0.39	4

[a]$\Delta T = T_{max}\varepsilon''$ (1 MHz) $- T_{max}\varepsilon''$ (100 Hz), frequency dispersion of the temperature of maximum from the imaginary part of dielectric permittivity.

decreased to a value below the experimental uncertainty of this procedure. After annealing, a cubic content was recovered in the sample. Thermal annealing and zero-field-cooling poled BNT-6BT results in depolarization that involves breaking of the ferroelectric long-range order and reestablishment of the relaxor state [16]. Accordingly, a marked decrease of the SSE intensity was observed after annealing [Fig. 1(c)], which resulted in an I_{SSE}/I_{CB} ratio of 0.88. This intensity change not only demonstrates that the cubic phase reappears as a result of thermal annealing, but it also shows that the cubic phase is reestablished at around 22%, which is a content similar as before poling [Fig. 1(f)].

These results have the following implications: A polar phase is present at all poling states, as evidenced by the ubiquitous presence of SSE. Nevertheless, a considerable amount of cubic phase is also present in unpoled and annealed samples (i.e., ground state), indicating that the ground state is not completely polarized. Instead, polar and cubic local symmetries coexist [Fig. 1(d) schematic]. This coexistence strongly suggests that the microstructure of the ground state of relaxors resembles the model of PNRs embedded in a cubic matrix rather than an assembly of nanometric ferroelectric domains separated only by domain walls.

The most striking feature is that the cubic content practically disappears when a ferroelectric state is induced by electric poling. This implies that the electric-field-induced transition from a relaxor into a ferroelectric state for this material is not solely caused by an alignment of dipoles in the direction of the applied electric field. The local symmetry change in the cubic phase indicates that PNRs grow at the expense of the cubic nonpolar matrix. The electric-field-induced breaking of the local cubic symmetry enables percolation of polarization throughout the whole structure and the establishment of a ferroelectric state.

Next, the consequences of electric poling on the local structure of compositions BNT-1BT, BNT-4BT, and BNT-15BT are discussed in order to correlate the local structural features with the macroscopic electric properties of ceramics with different barium content. Their ^{23}Na NMR spectra (not shown) resemble those of BNT-6BT (Fig. 1) except for different I_{SSE}/I_{CB} ratios and SSE widths. Table I collects these values before and after poling. Based on them and with the aid of Eq. (2), the percentage of the cubic phase was determined as a function of poling state for each composition and plotted in Fig. 2.

Note that both BNT-1BT and BNT-4BT exhibit a behavior similar to BNT-6BT: A cubic phase present before poling vanishes as a consequence of electric poling and is reestablished after annealing and zero-field cooling. As BNT-6BT, these compositions also exhibit relaxor features in the unpoled state [35,37], implying that the relaxor behavior is attributed to the observed cubic phase. This relation is further supported by the fact that BNT-15BT, a composition which does not display marked relaxor features, did not exhibit a considerable amount of a cubic phase.

We are also interested in comparing the local structure of these relaxor ferroelectrics to their macroscopic properties. Therefore, we contrast the amount of cubic phase present with the frequency dispersion of dielectric permittivity (Fig. 2). The relative amount of the cubic phase in the unpoled state varied

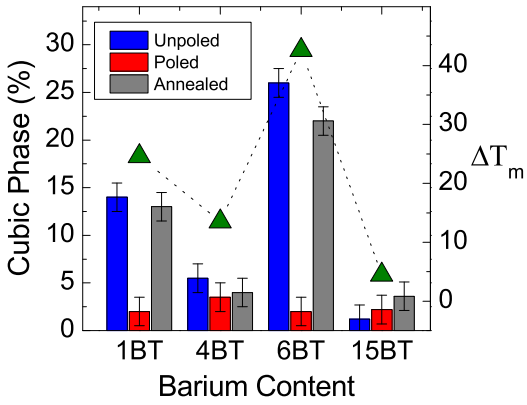

FIG. 2. (Color online) Relative amount of cubic phase for BNT-xBT as a function of barium content and poling state as contrasted to the frequency dependence of temperature of the permittivity's maximum ΔT_m (right axis, green triangles).

with barium content. BNT-6BT is featured by the highest cubic content, followed by BNT-1BT, and to a lesser extent by BNT-4BT. This trend can be compared to the intensity of relaxor features from each composition. An important characteristic of the relaxor state is the shift of the permittivity's maximum towards higher temperatures with increasing measuring frequency [44]. This shift is represented by $\Delta T_m = T_m(f_{\text{high}}) - T_m(f_{\text{low}})$, and the corresponding values are collected in Table I. The frequency dispersion of the temperature of $\varepsilon''_{\text{max}}$ follows the same trend observed for the amount of cubic phase, i.e., BNT-6BT > BNT-1BT > BNT-4BT.

These results strongly suggest that the coexistence of a cubic and a polar phase for the ground state of relaxors together with the polarization of the cubic matrix as a consequence of electric poling are not special features of BNT-6BT, but rather a general property of all BNT-xBT compositions with relaxor character.

Further information about the local structure of the polar phase can be extracted from the SSE. According to Eq. (1), the width of the SSE is a direct measure for V_{ZZ} and its distribution, and has, therefore, a direct connection to the local symmetry of PNRs. Consequently, an alteration in the local symmetry of the polar phase is expected to impact it. The full width at half maximum (FWHM) of the SSE for each composition is listed in Table I as a function of poling state. The width of the SSE did not change significantly with electric poling for the investigated BNT-xBT compositions, underpinning the hypothesis that the local structure of the polar phase (PNRs) did not change due to field cooling. This observation implies that the breaking of the macroscopic cubic symmetry upon electric poling [24,35] is not related to local structural changes in the polar phase. Rather, it indicates that the polar phase exhibits the same local structure in PNRs as well as in ferroelectric domains. Hence, we propose that the ferroelectric long-range order has its origin in the growth of the coherence length and the size of PNRs rather than in their local symmetry change.

In summary, the coexistence of a cubic and a polar phase was demonstrated in relaxor ferroelectric materials with BNT-xBT composition by means of quadrupolar ^{23}Na nuclear magnetic resonance. The coexistence of these local symmetries in the ground state of relaxors supports a picture for their microstructure that resembles one of PNRs embedded in a cubic nonpolar matrix. Moreover, the local symmetry of the polar phase does not change upon electric poling. This feature might indicate that PNRs and ferroelectric domains have the same local structure. We were also able to demonstrate that an electric-field-induced phase transformation occurs in the cubic matrix, which becomes polarized and adopts the local structure of nearby PNRs. We anticipate that these observations will help clarify the structure of both bismuth as well as lead-containing relaxor ferroelectrics and therefore give insight into the origin of relaxor features. Precise knowledge of the local structure will furthermore support the modeling of relaxor properties. Additionally, we expect these findings will stimulate further works on testing the applicability of theories developed for classical relaxors on lead-free systems.

Financial support by the Deutsche Forschungsgemeinschaft in the framework SFB-595 "Electric Fatigue in Functional Materials" is gratefully acknowledged. We thank Dr. Nikola Novak for helpful discussion.

[1] L. E. Cross, Ferroelectrics **76**, 241 (1987).
[2] Z. G. Ye, Key Eng. Mater. **155-156**, 81 (1998).
[3] V. V. Shvartsman and D. C. Lupascu, J. Am. Ceram. Soc. **95**, 1 (2012).
[4] A. A. Bokov and Z. G. Ye, J. Mater. Sci. **41**, 31 (2006).
[5] G. Schmidt, H. Arndt, G. Borchhardt, J. von Cieminski, T. Petzsche, K. Borman, A. Sternberg, A. Zirnite, and V. A. Isupov, Phys Status Solidi A **63**, 501 (1981).
[6] D. Viehland, J. F. Li, S. J. Jang, L. E. Cross, and M. Wuttig, Phys. Rev. B **43**, 8316 (1991).
[7] V. Westphal, W. Kleemann, and M. D. Glinchuk, Phys. Rev. Lett. **68**, 847 (1992).
[8] E. V. Colla, E. Y. Koroleva, N. M. Okuneva, and S. B. Vakhrushev, Phys. Rev. Lett. **74**, 1681 (1995).
[9] A. Levstik, Z. Kutnjak, C. Filipič, and R. Pirc, Phys. Rev. B **57**, 11204 (1998).
[10] R. Blinc, V. Laguta, and B. Zalar, Phys. Rev. Lett. **91**, 247601 (2003).
[11] I. K. Jeong, T. W. Darling, J. K. Lee, T. Proffen, R. H. Heffner, J. S. Park, K. S. Hong, W. Dmowski, and T. Egami, Phys. Rev. Lett. **94**, 147602 (2005).
[12] N. Novak, R. Pirc, M. Wencka, and Z. Kutnjak, Phys. Rev. Lett. **109**, 037601 (2012).
[13] G. Burns and F. H. Dacol, Solid State Commun. **48**, 853 (1983).
[14] D. Fu, H. Taniguchi, M. Itoh, S. Koshihara, N. Yamamoto, and S. Mori, Phys. Rev. Lett. **103**, 207601 (2009).
[15] Z.-G. Ye and H. Schmid, Ferroelectrics **145**, 83 (1993).
[16] W. Jo, S. Schaab, E. Sapper, L. A. Schmitt, H.-J. Kleebe, A. J. Bell, and J. Rödel, J. Appl. Phys. **110**, 074106 (2011).
[17] R. Dittmer, W. Jo, J. Rödel, S. Kalinin, and N. Balke, Adv. Funct. Mater. **22**, 4208 (2012).

[18] G. O. Jones and P. A. Thomas, Acta Crystallogr., Sect. B **58**, 168 (2002).
[19] S. Gorfman and P. A. Thomas, J. Appl. Crystallogr. **43**, 1409 (2010).
[20] T. Takenaka, K. Maruyama, and K. Sakata, Jpn. J. Appl. Phys. **30**, 2236 (1991).
[21] R. Ranjan and A. Dviwedi, Solid State Commun. **135**, 394 (2005).
[22] J. E. Daniels, W. Jo, J. Rödel, and J. L. Jones, Appl. Phys. Lett. **95**, 032904 (2009).
[23] R. Garg, B. N. Rao, A. Senyshyn, P. S. R. Krishna, and R. Ranjan, Phys. Rev. B **88**, 014103 (2013).
[24] H. Simons, J. Daniels, W. Jo, R. Dittmer, A. Studer, M. Avdeev, J. Rödel, and M. Hoffman, Appl. Phys. Lett. **98**, 082901 (2011).
[25] I. Levin and I. M. Reaney, Adv. Funct. Mater. **22**, 3445 (2012).
[26] J. Kreisel, P. Bouvier, B. Dkhil, P. A. Thomas, A. M. Glazer, T. R. Welberry, B. Chaabane, and M. Mezouar, Phys. Rev. B **68**, 014113 (2003).
[27] G. Xu, G. Shirane, J. R. D. Copley, and P. M. Gehring, Phys. Rev. B **69**, 064112 (2004).
[28] D. J. Goossens, ISRN Mater. Sci. **2013**, 107178 (2013).
[29] W. Ge, C. Luo, C. P. Devreugd, Q. Zhang, Y. Ren, J. Li, H. Luo, and D. Viehland, Appl. Phys. Lett. **103**, 241914 (2013).
[30] A. Abragam, *The Principles of Nuclear Magnetism* (Clarendon, Oxford, U.K., 1970).
[31] C. P. Slichter, *Principles of Magnetic Resonance* (Springer, Berlin, 1978).
[32] B. Zalar, V. V. Laguta, and R. Blinc, Phys. Rev. Lett. **90**, 037601 (2003).
[33] I. P. Aleksandrova, Y. N. Ivanov, A. A. Sukhovsky, and S. B. Vakhrushev, Phys. Solid State **48**, 1120 (2006).
[34] I. P. Aleksandrova, A. A. Sukhovsky, Y. N. Ivanov, Y. E. Yablonskaya, and S. B. Vakhrushev, Ferroelectrics **378**, 16 (2009).
[35] F. Craciun, C. Galassi, and R. Birjega, J. Appl. Phys. **112**, 124106 (2012).
[36] F. Cordero, F. Craciun, F. Trequattrini, E. Mercadelli, and C. Galassi, Phys. Rev. B **81**, 144124 (2010).
[37] J. E. Daniels, W. Jo, J. Rödel, D. Rytz, and W. Donner, Appl. Phys. Lett. **98**, 252904 (2011).
[38] S.-T. Zhang, A. B. Kounga, E. Aulbach, H. Ehrenberg, and J. Rödel, Appl. Phys. Lett. **91**, 112906 (2007).
[39] H. J. Jakobsen, J. Skibsted, H. Bildsøe, and N. C. Nielsen, J. Magn. Reson. **85**, 173 (1989).
[40] A. Samoson, Chem. Phys. Lett. **119**, 29 (1985).
[41] R. Blinc, A. Gregorovič, B. Zalar, R. Pirc, and S. G. Lushnikov, Phys. Rev. B **61**, 253 (2000).
[42] See Supplemental Material at http://link.aps.org/supplemental/10.1103/PhysRevB.90.220104 for derivation of Eq. (2) and comparison between the spinning sidebands envelope of unpoled BNT-6BT and $NaNO_2$ as reference sodium salt.
[43] C. Jäger, G. Kunath, P. Losso, and G. Scheler, Solid State Nucl. Magn. Reson. **2**, 73 (1993).
[44] D. Viehland, S. J. Jang, L. E. Cross, and M. Wuttig, J. Appl. Phys. **68**, 2916 (1990).